WHAT MEASUREMENTS OF ENERGY TRANSFER ACROSS NON-COVALENT CONTACTS IN PROTEINS REVEAL ABOUT THE ENERGY LANDSCAPE

Humanath Poudel and David M. Leitner[*]

Department of Chemistry, University of Nevada, Reno, NV 89557, USA

* Email address: dml@unr.edu

Abstract

Determining rates of energy transfer across non-covalent contacts in a protein can provide information about dynamics of the contact at equilibrium. We investigate the relation between rates of energy transfer across polar contacts and contact dynamics for the WW domain, dominated by β-strands, and compare with previous results for the helical villin headpiece subdomain, HP36. Overall, rates of energy transfer across hydrogen bonded contacts are found to be inversely proportional to the variance of the length of the contact. Due to the proportionality, change in dynamics of a non-covalent contact, and entropy associated with the dynamics, arising from change in state of the protein or mutation can be estimated from the measurement of change in the rate of energy transfer across the contact.

1.   Introduction

What can information about rates of energy transfer across non-covalent contacts in a protein tell us about the underlying energy landscape? Time-resolved vibrational spectroscopic studies are providing ever more insight into vibrational dynamics and energy flow in proteins [1-7] and that information may provide insights into at least local features of the landscape. Rates of energy transfer across contacts between different chemical groups in proteins are not only related to protein structure but also to the dynamics of the protein. More specifically, the rate of energy transfer across a non-covalent contact depends both on the nature of the contact and fluctuations in its length [8-16]. The equilibrium fluctuations are determined by local regions of the energy landscape [17-19] that the molecule samples during the period of time, typically tens of picoseconds, the molecule is probed. We thus get a snapshot of how rigid or fluxional a protein is in the region of a non-covalent contact that is studied. If different states of the protein are probed, e.g., active and inactive [20, 21], or if different mutants are studied [22], differences in rates of energy transfer across non-covalent contacts provide information about differences in dynamics and entropy associated with the dynamics for different states or mutants. In this Article, we further examine connections between rates of vibrational energy transfer across non-covalent contacts in proteins and the dynamics of the contact. We focus on hydrogen bonded contacts and compare the relation between rates of energy transfer across hydrogen bonded contacts of α-helices with hydrogen bonded contacts across β-strands.

In previous work we examined vibrational energy transfer across hydrogen bonds of α-helices, where a detailed study of the helical protein HP36 (Fig. 1) was carried out [9] to better understand contributions of polar and non-polar contacts in proteins to energy transport, both of which contribute to the overall anisotropic flow of energy in these molecules [23-37]. Energy flow

mediates rates of chemical reactions in proteins and other molecules [38-58]. The results of the HP36 study indicated a proportionality between rates of energy transfer across hydrogen-bonded contacts stabilizing α-helices and the inverse of the variance of the length of the contact at equilibrium. The trends found for the α-helices of HP36 have also been found for the α-helices of other proteins, including two G-protein coupled receptors (GPCRs) [20, 21]. The proportionality between rates of vibrational energy transfer across hydrogen bonds and dynamics of the contact has been found to be different for some other hydrogen bonded contacts. It is therefore worthwhile investigating hydrogen bonds across β-strands, to see how any trends compare with those for hydrogen bonds of α-helices. We examine this relation for the WW domain (Fig. 2), a small protein with a large fraction of residues in β-strands.
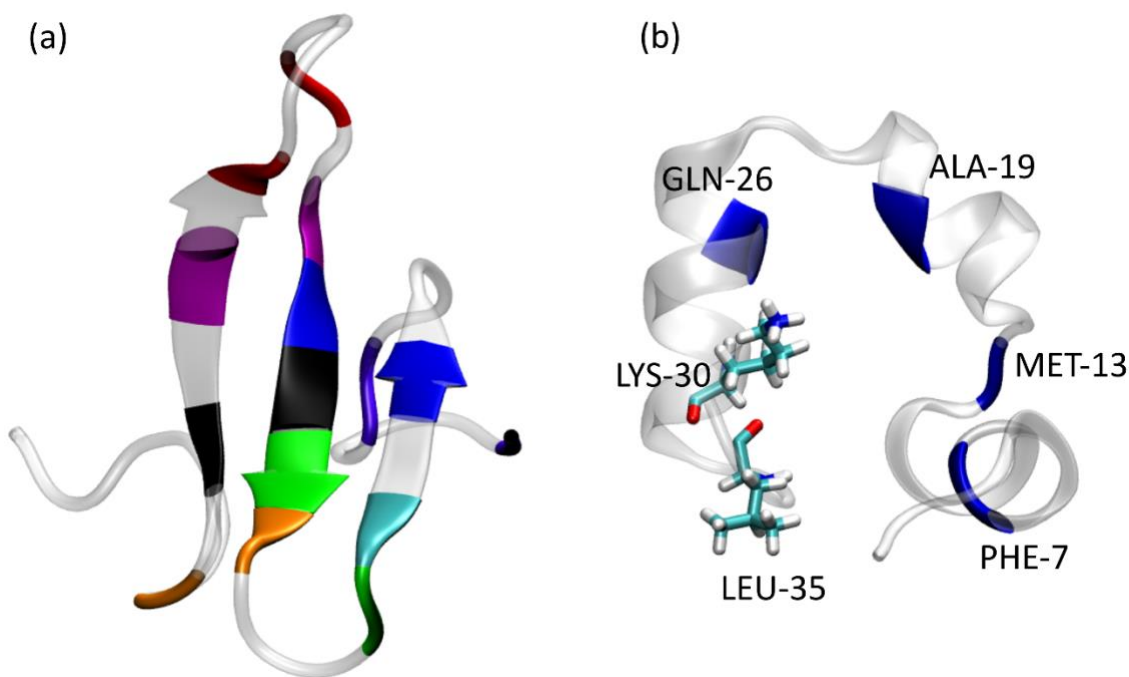

Figure 1. (a) The location of polar contacts of the WW domain. Each contact is highlighted with a unique color code listed in Table 1. Note that green is used for Asn22, which is involved in 2 contacts. (b) The location of polar contacts of HP36, other than those that stabilize α-helices. All contacts are backbone-backbone, with the exception of Lys30-Leu35, which involves the Lys30 sidechain, shown in the figure.

3

We study vibrational energy transport in the WW domain by computing energy exchange networks (EENs) using an approach and program developed by Yamato and coworkers [59, 60] where energy currents between residue pairs are computed in terms of energy flux time correlation functions using data from MD simulations. The energy current between a residue pair is proportional to the rate of energy transfer between the residues. The computational approach developed by Yamato and coworkers generates values of energy currents between residues based on the results of equilibrium molecular dynamics (MD) simulations. The same simulation data can also be used to compute fluctuations in the length of hydrogen bonds at equilibrium, so that the corresponding energy current can be paired with the dynamics using the same trajectory and the results compared. We have carried out this analysis for small proteins, such as HP36 [9], and relatively large membrane-bound proteins, such as GPCRs [16, 20, 21]. For polar and non-polar contacts, we have found an inverse proportionality between energy currents, and thus rates of energy transfer, across the contact and the variance of the contact length. This relation also holds for contacts between protein and water [11, 61], which also contribute to energy transport [33, 34, 62, 63]. The constant of proportionality for non-polar contacts is typically smaller than for polar contacts. One finds, however, some difference in rates of energy transfer across hydrogen bonds along an α-helix and, in some cases, other hydrogen bonds [9]. Examining hydrogen bonds forming β-strands is therefore worthwhile.

In Sec. 2.1 we summarize the computational methods used for the study of energy transfer across polar and non-polar contacts of the WW domain. In Sec. 2.2 we discuss from a theoretical perspective the relation between rates of energy transfer across non-covalent contacts and dynamics of the contact. In Section 3 we present and discuss results for the WW domain and compare with previous results reported for HP36. We conclude in Sec. 4.

2. Theoretical and computational methods

2.1. Computational methods

We obtained the initial structure of the WW domain from the Protein Data Bank entry 1E0M [64]. The structure was simulated using the AMBER ff14SB[65] forcefield in an octahedral box with a radius of 10 Å. The system was solvated using 3717 TIP3P[66] water molecules. All molecular dynamics simulations were performed using the AMBER16 MD[67] software package. Na^+ and Cl^- ions were added with a final concentration of 0.15 M NaCl. The system was energy minimized for 5000 steps using a force constant 50 (kcal mol^{-1})/Å^2 in all protein atoms. The second minimization of 5,000 steps was performed by constraining the protein heavy atoms using the same force constant and relaxing the hydrogen atoms. Finally, the system was minimized for 10,000 steps with a force constant of 2 (kcal mol^{-1})/Å^2 in protein heavy atoms. For the minimization, a non-bonded cutoff of 9 Å was employed for the particle-particle long-range interactions.

The initial velocities of atoms corresponding to the Maxwell-Boltzmann distributions were generated with a starting temperature of 0.1 K and the system was heated up to 300 K for a ns. An additional ns heating was performed holding temperature at 300 K. The Berendsen[68] thermostat was applied in the heating simulation under the canonical ensemble. The system was integrated every 2 fs. The SHAKE algorithm was applied to constrain the bonds containing hydrogens. Electrostatic interactions were accounted for under the particle mesh Ewald method [69].

The first equilibration simulation was performed for 2 ns under an isobaric-isothermal (NPT) ensemble with an integration time of 2 fs. A force constant of 2 (kcal mol^{-1})/Å^2 was applied to the protein heavy atoms in the equilibrium simulations. The second equilibration simulation was performed for 2 ns under an NPT ensemble without any positional constraints on protein atoms.

The time constants for the thermostat and barostat were selected as 1 ps. Finally, a production simulation of 100 ns was performed under an NPT ensemble. In this simulation, we saved the trajectory files every 1 ns for the later microcanonical (NVE) simulations. We simulated a total of 50 NVE simulations taking the trajectories from 51 to 100 ns. Each NVE simulation was allowed to evolve for 500 ps with an integration time of 0.5 fs. In the NVE simulations, the velocities of atoms were saved every 1 fs, and coordinates were saved every 5 fs. To reduce the energy drift in the NVE simulation, an Ewald sum tolerance of 10^{-7} was applied.

Energy Exchange Networks, EENs, computed using the CUrrent calculation for Proteins (CURP) version 1.2.1 developed by Yamato and coworkers [59], are convenient for this study since rates of energy transfer and contact dynamics can be computed using the same trajectory. A total of 50 CURP calculations were performed and a statistical average was computed for each state to compute EENs. Details of the CURP program can be found in Ref. [59] and [8] and application to as HP36 is described in Ref. [9], and the same approach is used here.

For the WW domain, the same criterion used in the prior study of HP36 [9] was adapted for the selection of hydrogen bonded polar contacts. A hydrogen bond is defined as A–H⋯O, where A is either oxygen or nitrogen. The distance of H⋯O is less than 2.8 Å and the angle AHO $\geq 150°$. We only included the hydrogen bonds that meet the given criterion 99 % of the time. The variance in the length, r, of the hydrogen bond H⋯O is computed as $\langle \delta r^2 \rangle = \langle (r - \langle r \rangle^2) \rangle$ where $\langle r \rangle$ is the average distance of H⋯O within each microcanonical simulation, where G is computed.

2.2. Energy transfer across non-covalent contacts and relation to contact dynamics

We consider the relation between the energy current, G, across a non-covalent contact, which is proportional to the rate of energy transfer, and the variance of the length of the contact, $\langle \delta r^2 \rangle^{-1}$. We have argued [10, 61] and shown in earlier work [9, 11, 13] that for many polar and non-polar contacts they are related as $G \propto \langle \delta r^2 \rangle^{-1}$. Here we present a different argument to understanding this proportionality.

We can picture the contact between chemical groups in the protein, which in turn are coupled to other chemical groups via a wide range of interactions, some covalent and other non-covalent contacts. In the harmonic approximation we take all contacts to be represented by springs with force constants, F_j, as depicted schematically in Fig. 2(a). The non-covalent contact of interest is represented by a spring with force constant, f.
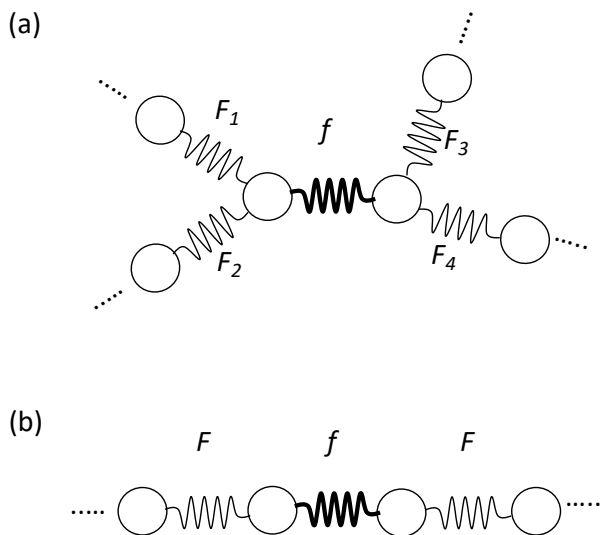

Figure 2. Schematic plot of polar or non-polar contact, represented by thickened spring with force constant, f, and other nearby contacts. In (a) other chemical groups interact with contact via random forces, F_1, F_2, etc. In (b) the chemical groups in contact with force constant, f, are in turn in contact with other groups represented by force constant, F.

In the initial state, there is excess energy in one of the chemical groups at one end of the contact with force constant, f. The chemical group is effectively in a harmonic oscillator potential with force constant, f, subject to random forces from all the other oscillators in the system. This can be represented as an Ornstein-Uhlenbeck process [70]. In this case, we have a particle subject to a harmonic force with force constant, f, in a Brownian environment with friction coefficient, ξ. The relaxation time, τ, for such a particle is $\tau = \xi/f$ [70]. This relaxation time, the time for the pulled spring to settle to equilibrium, is of the order of the time for the energy to travel to the chemical group to which the initially excited chemical group is interacting via the spring with force constant, f. The energy transfer time is thus comparable to τ. Since the equilibrium average of the variance of the length of the non-covalent contact, $\langle \delta r^2 \rangle$, is inversely proportional to the force constant, $\langle \delta r^2 \rangle = k_B T/f$, where k_B is Boltzmann's constant and T is temperature, we find that the rate of energy transfer, w, across the non-covalent contact varies as $\langle \delta r^2 \rangle^{-1}$ and is given by $w = \tau^{-1} = f\xi^{-1} = k_B T \xi^{-1} \langle \delta r^2 \rangle^{-1}$, so that w is proportional to $\langle \delta r^2 \rangle^{-1}$.

There is an interesting connection between this argument and a derivation by Stock [15] that also supports the proportionality between the rate of energy transfer across the non-covalent contact and $\langle \delta r^2 \rangle^{-1}$. That argument is based on the model depicted in Fig. 2(b). There the chemical groups forming the contact are bonded to other chemical groups by covalent bonds represented by spring constant F on each side, where $F \gg f$. The energy transfer rate is then found to be approximately given by $w = 2k_B T \pi^{-1} F^{-1/2} \langle \delta r^2 \rangle^{-1}$ [15]. This is analogous to the result above where the friction coefficient, ξ, is understood to be related to the spring constants, F, between the chemical groups forming the contact and other chemical groups.

There are useful consequences to the proportionality between rates of energy transfer across a contact, which can be measured [3, 6], and fluctuations in the length of the contact. When

the proportionality holds, we can estimate changes in dynamics of the contact and associated entropy if changes in rates of energy transfer during the transition from one state to another are measured. This can be seen as follows: At fixed temperature the change in entropy, $\Delta S = S_2 - S_1$, associated with change in dynamics of the non-covalent contact going from state 1 to 2, with change in force constant from f_1 to f_2 is $\Delta S = \frac{k_B}{2} \ln\left(\frac{f_1}{f_2}\right)$ in harmonic approximation. If G_1 and G_2 are proportional to the rate of energy transfer across a non-covalent contact in state 1 and state 2, respectively, then the change in entropy upon activation associated with a change in the dynamics of the contact is given by[10, 61, 71] $\Delta S = \frac{k_B}{2} \ln\left(\frac{G_1}{G_2}\right)$.

3.   Results and Discussion

In an earlier study we determined for the hydrogen bonded contacts of HP36 the variation of G with $\langle \delta r^2 \rangle^{-1}$. Those results, which were smoothed for clarity as described in Ref. [9], are plotted in Fig. 3. Results for the WW domain are also smoothed for clarity as in Ref. [9]. The hydrogen bonds along the α-helices of HP36, indicated in Fig. 1, are plotted in magenta. Data for other hydrogen bonds, not those stabilizing the α-helices, are plotted in blue. Almost all the data plotted in blue correspond to the Lys30-Leu35 contact, formed between the side chain of Lys30 and backbone of Leu35 [9]. Linear fits to the data are also indicated in Fig. 3. We find for the points plotted in magenta a fit of $G = 0.019\langle \delta r^2 \rangle^{-1} + 9.5$, ($R^2$ value of 0.96). For the points plotted in blue we find G = $0.0048\langle \delta r^2 \rangle^{-1} + 7.3$, ($R^2$, 0.77).

In subsequent studies, we have found that for hydrogen bonds stabilizing α-helices of other proteins, including transmembrane proteins β2 adrenergic receptor and GLP1, both G-protein

coupled receptors (GPCRs), the proportionality between G and $\langle \delta r^2 \rangle^{-1}$ is close to what we have found for the hydrogen bonds along the helices of HP36 [20, 21]. There appears to be a universality for hydrogen bonds stabilizing α-helices. That is not necessarily the case for other hydrogen bonded contacts. For the side chain-backbone contact represented by the data plotted in blue in Fig. 3, the proportionality is different.
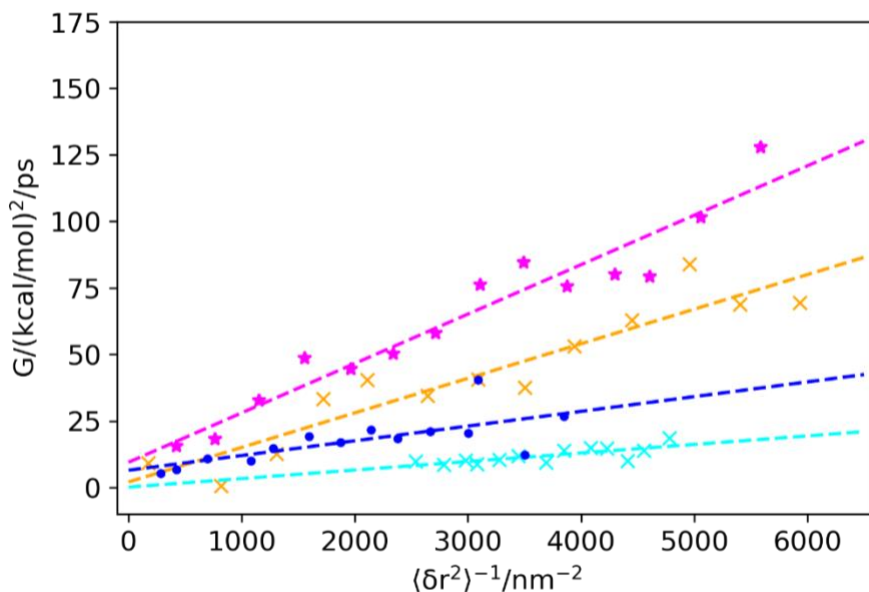

Figure 3. G vs $\langle \delta r^2 \rangle^{-1}$ hydrogen bonds of HP36 (magenta and blue) and the WW domain (orange and cyan). Data for HP36 are taken from Ref. [9]. Results plotted in magenta correspond to hydrogen bonds along α-helices. Data plotted in blue correspond to other hydrogen bonds of HP36 (see text). Linear fits plotted through the data are as follows: magenta: $G = 0.019\langle \delta r^2 \rangle^{-1} + 9.5$, ($R^2$ is 0.96); orange: $G = 0.013\langle \delta r^2 \rangle^{-1} + 1.9$, ($R^2$ is 0.94); blue: $G = 0.0048\langle \delta r^2 \rangle^{-1} + 7.3$, ($R^2$ is 0.77); cyan: $G = 0.0032\langle \delta r^2 \rangle^{-1} + 0.5$, ($R^2$ is 0.76).

We turn now to the results for the WW domain. The data for WW domain, shown in orange and cyan, break into two linear trends. Data for most of the contacts, listed in Table 1, are plotted in orange, where a linear fit gives $G = 0.013\langle \delta r^2 \rangle^{-1} + 1.9$, ($R^2$, 0.94). All contacts are backbone-backbone and represent contacts between different structural elements, including contacts between two β-strands, two loops and a β-strand with a turn, as well as a loop and coil. Despite the wide

range of structural elements linked by these backbone-backbone hydrogen bonded contacts, the variation in the rate of energy transfer as a function of fluctuation in the length of the contact is similar. The constant of proportionality between the rate of energy transfer and the inverse of the variance of the length of the contact is about 2/3 the value for hydrogen bonds stabilizing α-helices.

For two of the contacts, both hydrogen bonds between β–strands, the constant of proportionality is smaller; a linear fit to the data yields, $G = 0.0032\langle \delta r^2 \rangle^{-1} + 0.5$, ($R^2$, 0.76). While they follow the expected proportionality between G and $\langle \delta r^2 \rangle^{-1}$, it is unclear why the two contacts exhibit relatively small G for a given $\langle \delta r^2 \rangle^{-1}$ compared to the others. Nevertheless, the main utility of the proportionality between G and $\langle \delta r^2 \rangle^{-1}$ is not so much the specific constant of proportionality but instead that G and $\langle \delta r^2 \rangle^{-1}$ are proportional, as that can be used to identify changes in dynamics and entropy associated with dynamics upon change of state or mutation, as discussed below.

Table 1: List of WW domain hydrogen bonded contacts, all backbone-backbone. Color of the contact in Fig. 1 is indicated as is (in parenthesis) the color of data plotted for the contact in Fig. 3. Structural elements containing residues forming the contact are also listed.

Residue i	Residue j	Color in Fig. 1 (Color in Fig. 3)	Structural elements containing residues
GLY7	HIE23	orange (orange)	loop-loop
ASP9	TYR21	black (cyan)	beta-beta
TYR11	TYR19	magenta (orange)	beta-beta
THR13	LYS17	red (orange)	loop-loop
TYR20	THR29	blue (orange)	beta-beta
ASN22	THR27	cyan (cyan)	beta-beta
ASN22	LYS26	green (orange)	beta-turn
PRO33	SER37	violet (orange)	loop-coil

We note that for all results for hydrogen bonded contacts plotted in Fig. 3, values of G for a given $\langle\delta r^2\rangle^{-1}$ are substantially larger than for non-polar contacts. We have found a linear variation of $G = 0.0020\langle\delta r^2\rangle^{-1}$ for van der Waals contacts of HP36 [9], and similar trends for van der Waals contacts of two GPCRs [20, 21].

Change of state of a protein, e.g., by binding a ligand, can lead to change in dynamics of the protein, which contributes thermodynamically to the transition between states [71-73]. We have examined changes in G and changes in $\langle\delta r^2\rangle^{-1}$ of contacts of two GPCRs for the transition from inactive to active state [20, 21]. Change in G can occur when a contact breaks due to local structural changes. However, we also find contacts that remain intact during activation and G changes due to change in dynamics of the contact [21]. One example is shown in Fig. 4 for a backbone-sidechain hydrogen bonded contact between Thr136 and Tyr171 of β_2 adrenergic receptor.
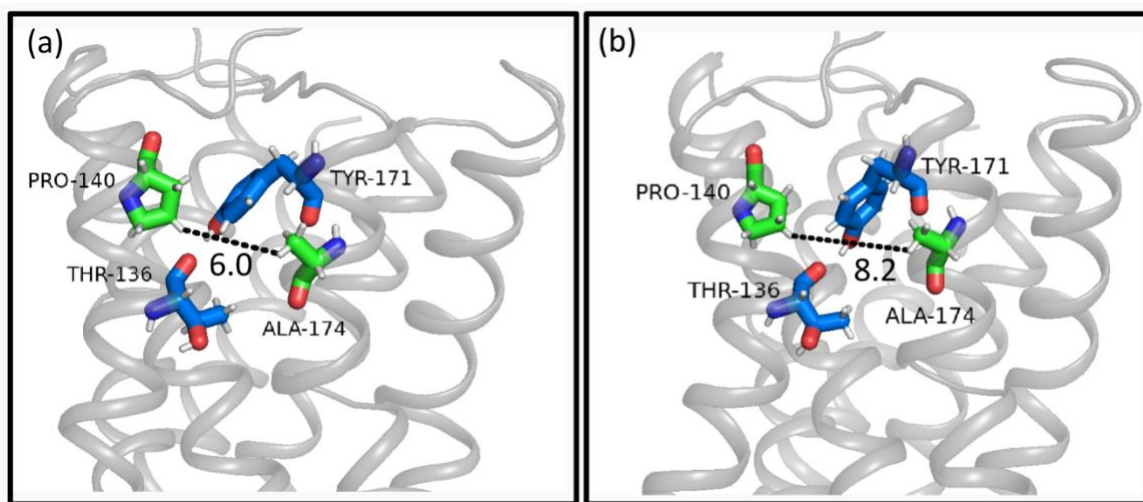

Figure 4. Polar contact Thr136-Tyr171 (blue) of β_2 adrenergic receptor in active (a) and inactive (b) states. The nearby contact Pro140-Ala174 is shown in green; the average minimum distance is smaller in the active state than inactive, restricting the motion of Thr136-Tyr171 in the active compared to inactive state. The average minimum distance between Pro140-Ala174 computed for each state is indicated (in Å).

Thr136-Tyr171 exhibits a relatively large change in dynamics between active and inactive states of β_2 adrenergic receptor, and, using Eq. (1), a correspondingly large entropy change, ΔS. We have found the ratio of G in the active to inactive state to be an unusually large 290, yielding $\Delta S \approx$ -21 J mol^{-1} K^{-1} for the transition from inactive to active state [21]. This ΔS, associated with change in dynamics of the contact, can be seen as a change in the spring constant associated with the contact during change in state. The change in spring constant occurs because of shifts in the average position of nearby residues, yielding a tighter contact in the active state. This is illustrated by snapshots of this contact for active and inactive states in Fig. 4(a) and 4(b), respectively, which reveal different packing around the contact by nearby residues in each state. The average minimum distance between the nearby residues Pro140 and Ala174, indicated in the figure, is computed to be 6.0 Å and 8.2 Å, respectively, in the active and inactive states [21]. The proximity of Pro140 and Ala174 in the active state restricts the motion of Tyr171, resulting in a tighter contact with Thr136 and on average larger G in the active state compared to the inactive state.

4.   Conclusions

We have examined the relation between rates of energy transfer across hydrogen bonded contacts and fluctuations in the length of the contact. We have focused on hydrogen bonded contacts along α-helices, between β-strands, and hydrogen bonds between less structured regions. In previous work we had identified what appears to be a universal proportionality between rates of energy transfer across hydrogen bonds that stabilize α-helices and fluctuations in the length of the bond [9]. That work focused on HP36, and the same proportionality has been since found for

transmembrane helices of two GPCRs [20, 21]. In this work, we have examined the same relation for hydrogen bonded contacts of the WW domain, where most stabilize contacts between β-strands.

For this computational study we obtain the energy current between residue-residue pairs using the CURP program developed by Yamato and coworkers [59], where the energy current is obtained from equilibrium MD simulations. The same trajectories can then be used to obtain information about fluctuations in the length of the contact and can be paired with the results for the energy current. For most of the hydrogen bonded contacts of the WW domain we find that the proportionality between the rate of energy transfer and the inverse of the variance of the length of the contact is somewhat smaller than the constant of proportionality we previously found for the hydrogen bonds that stabilize α-helices.

Rates of energy transfer across non-covalent contacts in proteins are currently being measured by time-resolved Raman and IR spectroscopy [1-7, 74, 75]. By relating rates of energy transfer to contact dynamics, measurement of energy transfer rates across non-covalent contacts for different states of a protein, or for different mutants, can be interpreted in terms of changes in dynamics and associated entropy. To estimate changes in dynamics and entropy associated with the dynamics it is important that the rate of energy transfer across a contact that is measured be proportional to the inverse of the variance of the length of the contact. We have seen this relation to hold for all the hydrogen bonds of the WW domain examined here, and for hydrogen bonds of a variety of other globular and membrane bound proteins in past studies [9-11, 13, 16, 20, 21, 61, 71]. Using this relation, measurement of rates of energy transfer across non-covalent contacts before and after a change of state of a protein or a mutation can be used to provide information

about local features of the underlying energy landscape, indicating more rigid or flexible motion when there is a change of state or mutation.

We have seen that the constant of proportionality between rates of energy transfer across a non-covalent contact and the inverse of the variance of contact length need not be the same for different hydrogen bonded contacts. We have discussed here a theory in which the constant of proportionality is expressed in terms of a spring constant between the chemical groups that are in contact and an effective friction coefficient due to interactions with the rest of the protein and its surroundings. It will be of interest in future work to provide a means to predict the constant of proportionality for a particular contact.

Data Availability

The data that support the findings of this study are available from the corresponding authors upon reasonable request.

References

[1] M. Mizuno, Y. Mizutani, Role of atomic contacts in vibrational energy transfer in myoglobin, Biophys. Rev., 12 (2020) 511 - 518.

[2] Y. Mizutani, Time-Resolved Resonance Raman Spectroscopy and Application to Studies on Ultrafast Protein Dynamics, Bull. Chem. Soc. Japan, 90 (2017) 1344 - 1371.

[3] Y. Mizutani, M. Mizuno, Time-resolved spectroscopic mapping of vibrational energy flow in proteins: Understanding thermal dffusion at the nanoscale, J. Chem. Phys., 157 (2022) 240901.

[4] N. Fujii, M. Mizuno, H. Ishikawa, Y. Mizutani, Observing vibrational energy flow in a protein with the spatial resolution of a single amino acid residue, J. Phys. Chem. Lett., 5 (2014) 3269−3273.

[5] T. Baumann, M. Hauf, F. Schildhauer, K.B. Eberl, P.M. Durkin, E. Deniz, J.G. Löffler, C.G. Acevedo-Rocha, J. Jaric, B.M. Martins, H. Dobbek, J. Bredenbeck, N. Budisa, Observation of Site-Resolved Vibrational Energy Transfer Using a Genetically Encoded Ultrafast Heater, Angew. Chem., 58 (2019) 2899 - 2903.

[6] E. Deniz, L. Valiño-Borau, J.G. Löffler, K.B. Eber, A. Gulzar, S. Wolf, P.M. Durkin, R. Kaml, N. Budisa, G. Stock, J. Bredenbeck, Through bonds or contacts? Mapping protein vibrational energy transfer using non-canonical amino acids, Nat. Comm., 12 (2021) 3284.

[7] J.G. Löffler, E. Deniz, C. Feid, V.G. Franz, J. Bredenbeck, Versatile vibrational energy sensors for proteins, Angewandte Chem., 134 (2022) e202200648.

[8] D.M. Leitner, T. Yamato, Mapping energy transport networks in proteins, in: A.L. Parrill, K.B. Lipkowitz (Eds.) Rev. Comp. Chem., John Wiley & Sons, Inc.2018, pp. 63 - 114.

[9] H. Poudel, K.M. Reid, T. Yamato, D.M. Leitner, Energy transfer across nonpolar and polar contacts in proteins: role of contact fluctuations, J. Phys. Chem. B, 124 (2020) 9852 - 9861.

[10] K.M. Reid, T. Yamato, D.M. Leitner, Scaling of rates of vibrational energy transfer in proteins with equilibrium dynamics and entropy, J. Phys. Chem. B, 122 (2018) 9331 - 9339.

[11] K.M. Reid, T. Yamato, D.M. Leitner, Variation of Energy Transfer Rates across Protein–Water Contacts with Equilibrium Structural Fluctuations of a Homodimeric Hemoglobin, J. Phys. Chem. B, 124 (2020) 1148 - 1159.

[12] T. Yamato, D.M. Leitner, Structure, dynamics, and energy flow that govern Heme protein functions: theory and experiments. Session 3SBA at the 57th BSJ Annual Meeting, Biophys. Rev., 12 (2020) 291 - 292.

[13] S. Buchenberg, D.M. Leitner, G. Stock, Scaling rules for vibrational energy transport in proteins, J. Phys. Chem. Lett., 7 (2016) 25 - 30.

[14] D.M. Leitner, S. Buchenberg, P. Brettel, G. Stock, Vibrational energy flow in the villin headpiece subdomain: Master equation simulations, J. Chem. Phys., 142 (2015) 075101.

[15] L. Valino-Borau, A. Gulzar, G. Stock, Master equation model to predict energy transport pathways in proteins, J. Chem. Phys., 152 (2020) 045103.

[16] H. Poudel, D.M. Leitner, Activation-Induced Reorganization of Energy Transport Networks in the B2 Adrenergic Receptor, J. Phys. Chem. B, 125 (2021) 6522 - 6531.

[17] D.J. Wales, Energy landscapes: some new horizons, Current Opinion in Structural Biology, 20 (2010) 3 - 10.

[18] D.W. Wales, Energy Landscapes, Cambridge University Press, Cambridge, 2003.

[19] S. Neelamraju, R.L. Johnston, J.C. Schön, A Threshold-Minimization Scheme for Exploring the Energy Landscape of Biomolecules: Application to a Cyclic Peptide and a Disaccharide, J. Chem. Theory Comput., 12 (2016) 2471 - 2479.

[20] H. Poudel, D.M. Leitner, Energy transport in class B GPCRs: Role of protein-water dynamics and activation, J. Phys. Chem. B, 42 (2022) 8362 - 8373.

[21] H. Poudel, D.M. Leitner, Locating dynamic contributions to allostery via determining rates of vibrational energy transfer, J. Chem. Phys., 158 (2023) 015101.

[22] S. Yamashita, M. Mizuno, D.P. Tran, H. Dokainish, A. Kitao, Y. Mizutani, Vibrational Energy Transfer from Heme through Atomic Contacts in Proteins, J. Phys. Chem. B, 122 (2018) 5877–5884.

[23] D.M. Leitner, Energy flow in proteins, Ann. Rev. Phys. Chem., 59 (2008) 233 - 259.

[24] X. Yu, D.M. Leitner, Vibrational energy transfer and heat conduction in a protein, J. Phys. Chem. B, 107 (2003) 1698 - 1707.

[25] X. Yu, D.M. Leitner, Anomalous diffusion of vibrational energy in proteins, J. Chem. Phys., 119 (2003) 12673 - 12679.

[26] X. Yu, D.M. Leitner, Heat flow in proteins: Computation of thermal transport coefficients, J. Chem. Phys., 122 (2005) 054902.

[27] D.M. Leitner, C. Hyeon, K.M. Reid, Water-mediated biomolecular dynamics and allostery, J. Chem. Phys., 152 (2020) 240901.

[28] L. Bu, J.E. Straub, Simulating vibrational energy flow in proteins: Relaxation rate and mechanism for heme cooling in cytochrome c, J. Phys. Chem. B, 107 (2003) 12339 – 12345.

[29] D.M. Leitner, J.E. Straub, Proteins: Energy, Heat and Signal Flow CRC Press, Taylor & Francis Group, Boca Raton, FL, 2010.

[30] D.E. Sagnella, J.E. Straub, Directed energy "funneling" mechanism for heme cooling following ligand photolysis or direct excitation in solvated carbonmonoxy myoglobin, J. Phys. Chem. B 105 (2001) 7057 – 7063.

[31] Y. Xu, D.M. Leitner, Communication maps of vibrational energy transport in photoactive yellow protein, J. Phys. Chem. A, 118 (2014) 7280 - 7287.

[32] Y. Xu, D.M. Leitner, Vibrational energy flow through the green fluorescent protein-water interface: Communication maps and thermal boundary conductance, J. Phys. Chem. B, 118 (2014) 7818 -7826.

[33] J.K. Agbo, R. Gnanasekaran, D.M. Leitner, Communication maps: Exploring energy transport through proteins and water, Isr. J. Chem., 54 (2014) 1065 - 1073.

[34] R. Gnanasekaran, J.K. Agbo, D.M. Leitner, Communication Maps Computed for Homodimeric Hemoglobin: Computational Study of Water-Mediated Energy Transport in Proteins, J. Chem. Phys., 135 (2011) 065103.

[35] T. Ishikura, T. Yamato, Energy transfer pathways relevant for long-range intramolecular signaling of photosensory protein revealed by microscopic energy conductivity analysis, Chem. Phys. Lett., 432 (2006) 533 – 537.

[36] K. Ota, T. Yamato, Energy exchange network model demonstrates protein allosteric transition: An application to an oxygen sensor protein, J. Phys. Chem. B, 123 (2019) 768 - 775.

[37] J.K. Agbo, Y. Xu, P. Zhang, J.E. Straub, D.M. Leitner, Vibrational energy flow across heme-cytochrome c and cytochrome c-water interfaces, Theor. Chem. Acc., 133 (2014) art. no. 1504.

[38] D.M. Leitner, Influence of quantum energy flow and localization on molecular isomerization in gas and condensed phases, Int. J. Quantum Chem., 75 (1999) 523 - 531.

[39] D.M. Leitner, Heat transport in molecules and reaction kinetics: The role of quantum energy flow and localization, Adv. Chem. Phys., 130B (2005) 205 - 256.

[40] S. Mondal, S. Keshavamurthy, Phase space perspective on a model for isomerization in an optical cavity, J. Chem. Phys., 159 (2023) 074106.

[41] S. Karmakar, S. Keshavamurthy, Intramolecular vibrational energy redistribution and the quantum ergodicity transition: a phase space perspective, Phys. Chem. Chem. Phys., 22 (2020) 11139 - 11173.

[42] S. Patra, S. Keshavamurthy, Classical-quantum correspondence in a model for conformational dynamics: Connecting phase space reactive islands with rare events sampling, Chem. Phys. Lett., 634 (2015) 1 - 10.

[43] D.M. Leitner, Quantum ergodicity and energy flow in molecules, Adv. Phys., 64 (2015) 445 - 517.

[44] D.M. Leitner, M. Gruebele, A quantum model of restricted vibrational energy flow on the way to the transition state in unimolecular reactions, Mol. Phys., 106 (2008) 433 - 442.

[45] J.K. Agbo, D.M. Leitner, D.A. Evans, D.J. Wales, Influence of vibrational energy flow on isomerization of flexible molecules: Incorporating non-RRKM kinetics in the simulation of dipeptide isomerization, J. Chem. Phys., 123 (2005) 124304.

[46] D.M. Leitner, B. Levine, J. Quenneville, T.J. Martinez, P.G. Wolynes, Quantum energy flow and trans stilbene photoisomerization: an example of a non-RRKM reaction, J. Phys. Chem., 107 (2003) 10706-10716.

[47] D.M. Leitner, P.G. Wolynes, Quantum energy flow during molecular isomerization, Chem. Phys. Lett., 280 (1997) 411-418.

[48] D.M. Leitner, Quantum localization and protein-assisted vibrational energy flow in cofactors, New J. Phys., 12 (2010) 085004.

[49] P. Antoniou, Z. Ma, P. Zhang, D.N. Beratan, S.S. Skourtis, Vibrational control of electron-transfer reactions: a feasibility study for the fast coherent transfer regime, Phys. Chem. Chem. Phys., DOI: 10.1039/C5CP00610D (2015).

[50] Z. Lin, C.M. Lawrence, D. Xiao, S.S. Skourtis, J.L. Sessler, D.N. Beratan, I.V. Rubtsov, Modulating unimolecular charge transfer by exciting bridge vibrations, J. Am. Chem. Soc., 131 (2009) 18060 - 18062.

[51] R. Kozlowski, J. Zhao, R.B. Dyer, Acceleration of catalysis in dihydrofolate reductase by transient, site-specific photothermal excitation, Proc. Natl. Acad. Sci. (USA), 118 (2021) e2014592118.

[52] M. Delor, P.A. Scattergood, I.V. Sazanovich, A.W. Parker, G.M. Greetham, A.J.H.M. Meijer, M. Towrie, J.A. Weinstein, Toward control of electron transfer in donor-acceptor molecules by bond-specific infrared excitation, Science, 346 (2015) 1492 - 1495.

[53] D.M. Leitner, Illuminating Fermi Resonances that Trigger Reaction in a Complex Molecule, Chem, 5 (2019) 256 - 257.

[54] M.J.B. S. Rafiq, P. J. Chirik, G. D. Scholes, Dinitrogen Coupling to a Terpyridine-Molybdenum Chromophore Is Switched on by Fermi Resonance, Chem, 5 (2019) 402 - 416.

[55] J.K. Agbo, D.M. Leitner, E.M. Myshakin, K.D. Jordan, Quantum energy flow and the kinetics of water shuttling between hydrogen bonding sites on trans-formanilide (TFA), J. Chem. Phys., 127 (2007) art. 064315, pp. 064311 – 064310

[56] J.P.T. Zaragoza, A.R. Offenbacher, S. Hu, J.P. Klinman, Temporal and spatial resolution of distal protein motions that activate hydrogen tunneling in soybean lipoxygenase, Proc. Natl. Acad. Sci. (USA), 120 (2023) e2211630120.

[57] T. Komatsuzaki, R.S. Berry, D.M. Leitner, Advancing Theory for Kinetics and Dynamics of Complex, Many-Dimensional Systems: Clusters and Proteins, Wiley, Hoboken, 2011.

[58] D.M. Leitner, Y. Matsunaga, C.-B. Li, T. Komatsuzaki, A. Shojiguchi, M. Toda, Non-Brownian Phase Space Dynamics of Molecules, the Nature of Their Vibrational States, and Non-RRKM Kinetics, Adv. Chem. Phys., 145 (2011) 83 - 122.

[59] T. Ishikura, Y. Iwata, T. Hatano, T. Yamato, Energy Exchange Network of Inter-Residue Interactions Within a Thermally Fluctuating Protein: A Computational Study, J. Comput. Chem., 36 (2015) 1709 - 1718.

[60] T. Yamato, T. Wang, W. Sugiura, O. Laprevote, T. Katagiri, Computational Study on the Thermal Conductivity of a Protein, J. Phys. Chem. B, 126 (2022) 3029 - 3036.

[61] D.M. Leitner, H.D. Pandey, K.M. Reid, Energy Transport across Interfaces in Biomolecular Systems, J. Phys. Chem. B, 123 (2019) 9507 - 9524.

[62] R. Gnanasekaran, Y. Xu, D.M. Leitner, Dynamics of Water Clusters Confined in Proteins: A Molecular Dynamics Simulation Study of Interfacial Waters in a Dimeric Hemoglobin, J. Phys. Chem. B, 114 (2010) 16989 - 16996.

[63] M. Heyden, Resolving anisotropic distributions of correlated vibrational motion in protein hydration water, J. Chem. Phys., 141 (2014) 22D509.

[64] M.J. Macias, V. Gervais, C. Civera, H. Oschkinat, Structural Analysis of WW Domains and Design of a WW Prototype, Nat Struct Biol 7(2000) 375 - 379.

[65] J. Wang, R.M. Wolf, J.W. Caldwell, P.A. Kollman, D.A. Case, Development and Testing of a General Amber Force Field, J. Comp. Chem., 25 (2004) 1157 - 1174.

[66] P.N. Mark, L. , Structure and Dynamics of the TIP3P, SPC, and SPC/E Water Models at 298 K, J. Phys. Chem. A, 105 (2001) 9954 - 9960.

[67] D.A. Case, R.M. Betz, D.S. Cerutti, T.E. Cheatham, T.A. Darden, R.E. Duke, T.J. Giese, H. Gohlke, A.W. Goetz, N. Homeyer, S. Izadi, P. Janowski, J. Kaus, A. Kovalenko, T.S. Lee, S. LeGrand, P. Li, C. Lin, T. Luchko, R. Luo, B. Madej, D. Mermelstein, K.M. Merz, G. Monard, H. Nguyen, H.T. Nguyen, I. Omelyan, A. Onufriev, D.R. Roe, A. Roitberg, C. Sagui, C.L. Simmerling, W.M. Botello-Smith, J. Swails, R.C. Walker, J. Wang, R.M. Wolf, X. Wu, L. Xiao, P.A. Kollman, AMBER 2016, University of California, San Francisco, DOI (2016).

[68] H.J.C. Berendsen, J.P.M. Postma, W.F. van Gunsteren, A. DiNola, J.R. Haak, Molecular Dynamics with Coupling to an External Bath, J. Chem. Phys., 81 (1984) 3684- 3690.

[69] T. Darden, D. York, L. Peterson, Particle mesh Ewald: An N log(N) method for Ewald sums in large systems, J. Chem. Phys., 98 (1993) 10089 - 10092.

[70] R. Zwanzig, Nonequilibrium statistical mechanics, Oxford University Press, Oxford, 2001.

[71] K.M. Reid, X. Yu, D.M. Leitner, Change in vibrational entropy with change in protein volume estimated with mode Grüneisen parameters, J. Chem. Phys., 154 (2021) 055012.

[72] A. Cooper, D.T.F. Dryden, Allostery without conformational change: A plausible model, Eur. Biophys. J., 11 (1984) 103 - 109.

[73] M. Post, B. Lickert, G. Diez, S. Wolf, G. Stock, Cooperative protein allosteric transition mediated by a fluctuating transmission network, J. Mol. Biol. , 434 (2022) art. 167679.

[74] S. Yamashita, M. Mizuno, Y. Mizutani, High suitability of tryptophan residues as a spectroscopic thermometer for local temperature in proteins under nonequilibrium conditions, J. Chem. Phys., 156 (2022) 075101.

[75] E.H. Backus, R. Bloem, R. Pfister, A. Moretto, M. Crisma, C. Toniolo, P. Hamm, Dynamical transition in a small helical peptide and its implication for vibrational energy transport, J. Phys. Chem. B, 113 (2009) 13405-13409.